https://doi.org/10.5194/amt-2019-405
Preprint. Discussion started: 14 November 2019

Atmospheric Measurement Techniques Discussions

An intercomparison of CH_3O_2 measurements by Fluorescence Assay by Gas Expansion and Cavity Ring–Down Spectroscopy within HIRAC (Highly Instrumented Reactor for Atmospheric Chemistry)

Lavinia Onel[1], Alexander Brennan[1], Michele Gianella[2], James Hooper[1], Nicole Ng[2], Gus Hancock[2], Lisa Whalley[1,3], Paul W. Seakins[1,3], Grant A. D. Ritchie[2], Dwayne E. Heard[1,3]

[1] School of Chemistry, University of Leeds, Leeds, LS2 9JT, UK
[2] Department of Chemistry, Physical and Theoretical Chemistry Laboratory, University of Oxford, Oxford, OX1 3QZ, UK
[3] National Centre for Atmospheric Science, University of Leeds, Leeds, LS2 9JT, UK

Correspondence to: Lavinia Onel (chmlo@leeds.ac.uk); Paul Seakins (p.w.seakins@leeds.ac.uk); Grant Ritchie (grant.ritchie@chem.ox.ac.uk); Dwayne Heard (d.e.heard@leeds.ac.uk)

Abstract

Simultaneous measurements of CH_3O_2 radical concentrations have been performed using two different methods in the Leeds HIRAC (Highly Instrumented Reactor for Atmospheric Chemistry) chamber at 295 K and in 80 mbar of a mixture of 3:1 He:O_2 and 100 mbar or 1000 mbar of synthetic air. The first detection method consisted of the indirect detection of CH_3O_2 using the conversion of CH_3O_2 into CH_3O by excess NO with subsequent detection of CH_3O by fluorescence assay by gas expansion (FAGE). The FAGE instrument was calibrated for CH_3O_2 in two ways. In the first method, a known concentration of CH_3O_2 was generated using the 185 nm photolysis of water vapour in synthetic air at atmospheric pressure followed by the conversion of the generated OH radicals to CH_3O_2 by reaction with CH_4/O_2. This calibration can be used for experiments performed in HIRAC at 1000 mbar in air. In the second method, calibration was achieved by generating a near steady-state of CH_3O_2 and then switching off the photolysis lamps within HIRAC and monitoring the subsequent decay of CH_3O_2 which was controlled via its self-reaction, and analysing the decay using second order kinetics. This calibration could be used for experiments performed at all pressures. In the second detection method, CH_3O_2 has been measured directly using Cavity Ring-Down Spectroscopy (CRDS) using the absorption at 7487.98 cm^{-1} in the $A \leftarrow X$ (ν_{12}) band with the optical path along the ~1.4 m chamber diameter. Analysis of the second-order kinetic decays of CH_3O_2 by self-reaction monitored by CRDS has been used for the determination of the CH_3O_2 absorption cross section at 7487.98 cm^{-1}, both at 100 mbar of air and at 80 mbar of a 3:1 He:O_2 mixture, from which $\sigma_{CH3O2} = (1.49 \pm 0.19) \times 10^{-20}$ cm^2 $molecule^{-1}$ was determined for both pressures. The absorption spectrum of CH_3O_2 between 7486 and 7491 cm^{-1} did not change shape when the total pressure was increased to 1000 mbar, from which we determined that σ_{CH3O2} is independent of pressure over the pressure range 100–1000 mbar in air. CH_3O_2 was generated in HIRAC using either the photolysis of Cl_2 with UV black lamps in the presence of CH_4 and O_2 or the photolysis of acetone at 254 nm in the presence of O_2. At 1000 mbar of synthetic air the correlation plot of $[CH_3O_2]_{FAGE}$ against $[CH_3O_2]_{CRDS}$ gave a gradient of 1.09 ± 0.06. At 100 mbar of synthetic air the gradient of the FAGE – CRDS correlation plot had a gradient of 0.95 ± 0.02 and at 80 mbar of 3:1 He:O_2 mixture the correlation plot gradient was 1.03 ± 0.05. These results provide a validation of the FAGE method to determine concentrations of CH_3O_2.

1 Introduction

Methyl peroxy (CH_3O_2) radicals are important intermediates during atmospheric oxidation (Orlando and Tyndall, 2012) and combustion chemistry (Zador et al., 2011), and are produced mainly by the oxidation of CH_4 and larger hydrocarbons followed by the termolecular reaction between the CH_3 radical, O_2 and a third body (Reaction R1).

$$CH_3 + O_2 + M \rightarrow CH_3O_2 + M \qquad (R1)$$

https://doi.org/10.5194/amt-2019-405
Preprint. Discussion started: 14 November 2019

Atmospheric Measurement Techniques Discussions

In environments influenced by anthropogenic NO_x emissions, CH_3O_2 predominantly reacts with NO to produce NO_2 and CH_3O (Reaction R2).

$$CH_3O_2 + NO \rightarrow CH_3O + NO_2 \quad (R2)$$

CH_3O subsequently reacts with O_2 (Reaction R3) to generate HO_2, which in turn oxidises another NO molecule to NO_2 (Reaction R4). The subsequent photolysis of NO_2 leads to the formation of tropospheric ozone, an important constituent of photochemical smog.

$$CH_3O + O_2 \rightarrow CH_2O + HO_2 \quad (R3)$$
$$HO_2 + NO \rightarrow OH + NO_2 \quad (R4)$$

In remote, clean environments, i.e. under low NO_x levels, CH_3O_2 is significantly removed by its self-reaction (Reaction R5) and the cross-reactions with HO_2 and other organic peroxy radicals (RO_2) (Tyndall et al., 2001).

$$CH_3O_2 + CH_3O_2 \rightarrow CH_3OH + CH_2O + O_2 \quad (R5a)$$
$$CH_3O_2 + CH_3O_2 \rightarrow CH_3O + CH_3O + O_2 \quad (R5b)$$

Recently the reaction of CH_3O_2 with OH was measured to be fast (Fittschen, 2019) and provides an additional loss route for CH_3O_2 under low NO_x conditions (Fittschen et al., 2014; Assaf et al., 2017). As CH_3O_2 is formed by the oxidation of CH_4, one of the most abundant tropospheric trace gases, as well as by the oxidation of other volatile organic compounds, it is predicted by numerical models to be the most abundant RO_2 species in the atmosphere. Although CH_3O_2 has not (yet) been selectively measured in the atmosphere, its concentration has been estimated using atmospheric models to peak at ~10^7 – 10^8 molecule cm^{-3} during the daytime (Whalley et al., 2010; Whalley et al., 2011; Whalley et al., 2018).

At present, CH_3O_2 is not measured selectively in the atmosphere by any direct or indirect method. The sum of HO_2 and all RO_2 species, $[HO_2] + \sum_i [RO_{2,i}]$, and separately, the sum of RO_2, $\sum_i [RO_{2,i}]$, have been measured in the atmosphere using a range of indirect methods. Onel et al. (2017a) presents an overview of these methods, such as the peroxy radical chemical amplifier (PERCA) (Cantrell et al., 1984; Hernandez et al., 2001; Green et al., 2006; Miyazaki et al., 2010; Wood et al., 2017), RO_x chemical conversion – CIMS (chemical ionisation mass spectrometry) (RO_xMAS) (Hanke et al., 2002) and RO_x chemical conversion – LIF (laser induced fluorescence) (RO_xLIF) (Fuchs et al., 2008; Whalley et al., 2013). RO_xLIF uses LIF detection of OH at low pressure, known as fluorescence assay by gas expansion (FAGE) and has been employed for partially speciated RO_2 detection, distinguishing between the sum of alkene, aromatic and long-chain alkane-derived RO_2 radicals and the sum of short-chain alkane-derived RO_2 radicals (Whalley et al., 2013; Whalley et al., 2018).

Many of the early laboratory studies of the CH_3O_2 radical reactions employed UV-absorption spectroscopy to monitor the $B \leftarrow X$ band centred around 240 nm, that is common to alkyl RO_2 species (Wallington et al., 1992; Tyndall et al., 2001). The similarity of the broad featureless UV-absorption spectra of RO_2 radicals made it challenging to distinguish between the individual RO_2 species, particularly in a mixture (Orlando and Tyndall, 2012). The sensitivity of UV-absorption spectroscopy is quite low, for example a minimum detectable absorption of 5×10^{-3}, corresponding to 4×10^{12} molecule cm^{-3} CH_3O_2 was reported (Sander and Watson, 1980). The $A \leftarrow X$ electronic transition of RO_2 in the near IR (NIR) displays more structured spectra than the UV region, allowing a selective identification of RO_2 radicals. However the $A \leftarrow X$ transition is weaker than the $B \leftarrow X$ transition and multipass arrangements have been used to improve the detection sensitivity. A step-scan Fourier

https://doi.org/10.5194/amt-2019-405
Preprint. Discussion started: 14 November 2019

Atmospheric Measurement Techniques Discussions

Transform Infrared spectrometer (Huang et al., 2007) operated using a multipass White cell has been used to detect a number of RO_2 species, including CH_3O_2, with a typical minimum detectable absorbance of ~ 1×10^{-4}, corresponding to a limit of detection (*LOD*) of ~ 1×10^{13} molecule cm^{-3} for most RO_2 species studied. The use of cavity ring-down spectroscopy (CRDS) further improves the sensitivity of the RO_2 detection due to the significantly longer pathlengths that can be realized and to the coupling of high performance NIR lasers, detectors and optical components. For example, an absorbance detection limit of less than 1×10^{-6} has been obtained by using cavity mirrors of a maximum reflectivity of 99.995% (Atkinson and Spillman, 2002).

The CRDS technique has been used under both ambient and jet-cooled conditions to provide insight into the molecular structure of CH_3O_2 and more complex RO_2, and to selectively measure [RO_2] in the laboratory (Sharp et al., 2008; Kline and Miller, 2014; Pushkarsky et al., 2000; Farago et al., 2013; Atkinson and Spillman, 2002; Sprague et al., 2013). Good agreement has been found between the experimental spectrum of CH_3O_2 in the range between ~7200–8600 cm^{-1} (~1.18–1.40 μm) measured using pulsed CRDS at typically 200 mbar of N_2:O_2 = 1.5:1.0 and theoretical predictions (Chung et al., 2007; Sharp et al., 2008). The origin band of the $A \leftarrow X$ transition has been located at 7382.8 cm^{-1} and a value of 2.7×10^{-20} cm^2 $molecule^{-1}$ has been estimated for the absorption cross section at this wavenumber (Pushkarsky et al., 2000; Chung et al., 2007). A weaker absorption band has been found at 7488 cm^{-1} and assigned to a transition involving the methyl torsion (ν_{12}) (Pushkarsky et al., 2000; Chung et al., 2007). By using the CH_3O_2 spectrum measured by Pushkarsky et al. (2000) from 7300–7700 cm^{-1}, which covers both the origin band and the band involving the methyl torsional mode, a value of ca. 1.0×10^{-20} cm^2 $molecule^{-1}$ is estimated for the maximum cross section for the ν_{12} transition, $\sigma_{max}(\nu_{12})$. A few years later, (Atkinson and Spillman, 2002) measured $\sigma_{max}(\nu_{12}) = (1.5 \pm 0.8) \times 10^{-20}$ cm^2 $molecule^{-1}$ at 27 mbar N_2:O_2 = 4:1 using continuous-wave (cw) CRDS. Very recent cw-CRDS studies reported $\sigma_{max}(\nu_{12}) = 2.2 \times 10^{-20}$ cm^2 $molecule^{-1}$ at 67 mbar of a He + O_2 mixture (Fittschen, 2019) and no dependence of $\sigma_{max}(\nu_{12})$ on pressure over the range from 67 to 133 mbar (Farago et al., 2013).

Recently we have developed a new method for the selective and sensitive detection of CH_3O_2 using the conversion of CH_3O_2 to CH_3O with excess NO followed by CH_3O detection by FAGE with laser excitation at *ca*. 298 nm (Onel et al., 2017b). The *LOD* for the method whilst sampling from atmospheric pressure is ~ 4.0×10^8 molecule cm^{-3} for a signal-to-noise ratio of 2 and 5 min averaging time; the *LOD* is reduced to ~ 1.0×10^8 molecule cm^{-3} by averaging over 1 hour. Therefore, the method has potential to be used in the measurement of atmospheric levels of CH_3O_2 in clean environments where [CH_3O_2] has been calculated to be a few 10^8 molecule cm^{-3} (Whalley et al., 2010; Whalley et al., 2011). As LIF is not an absolute method of detection, FAGE instruments require calibration. Two methods of calibration for CH_3O_2 have been used (Onel et al., 2017b): the 184.9 nm photolysis of water vapour in the presence of excess CH_4 and the kinetics of the second-order decay of CH_3O_2 via its self–reaction observed in the Highly Instrumented Reactor for Atmospheric Chemistry (HIRAC). Good agreement was found, *i.e*. the calibration factors obtained using the two methods had overlapping error limits at the 1σ level.

However, radicals are difficult to detect accurately and, particularly as FAGE is not an absolute and direct method, may be subject to systematic errors and, hence require validation using complementary methods. Recently we intercompared measurements of HO_2 concentrations by the indirect FAGE method and the direct and absolute CRDS method within HIRAC, and demonstrated good agreement, within 10% and 16% at 150 mbar and 1000 mbar, respectively (Onel et al., 2017b), which validates the FAGE method for HO_2. In this work, CH_3O_2 measurements by FAGE and CRDS within HIRAC are intercompared at 80 mbar for a mixture of 3:1 He:O_2 and at 100 mbar and 1000 mbar for air.

https://doi.org/10.5194/amt-2019-405
Preprint. Discussion started: 14 November 2019

Atmospheric Measurement Techniques Discussions

2 Experimental

2.1 CH_3O_2 generation in HIRAC

The HIRAC chamber (Glowacki et al., 2007) is constructed from 304 stainless steel and has an internal volume of ~2.25 m^3, the contents of which are homogenised by four mixing fans. Eight 50 mm diameter quartz tubes are mounted radially inside the chamber and extend along its ~2 m length. Each of the eight tubes house a UV lamp that is used to initiate chemical reactions. The lamps can be changed to different wavelength outputs depending on the chemical precursors to be used. The FAGE instrument is connected to the HIRAC chamber through an ISO-K160 flange with an O-ring compression fitting to allow the inlet distance from the wall of the chamber to be varied. The 380 mm long inlet allows the instrument to sample well away from the inner walls of the HIRAC chamber and avoid chemical processes at the metal surface. Because the FAGE system removes gas from the HIRAC chamber, a constant flow of synthetic air is introduced into the chamber to maintain a constant pressure. The CRDS setup is described in Sect. 2.3.

The experiments were conducted inside the HIRAC chamber at 295 K using three different pressure / gas mixtures. The first used 80 mbar total pressure of helium (BOC, >99.99 %) and oxygen (BOC, >99.999 %) in the ratio of $He:O_2$ = 3:1. The second and third mixtures both used synthetic air obtained by mixing oxygen with nitrogen (BOC, > 99.998 %) in the ratio $N_2:O_2$ = 4:1 at 100 and 1000 mbar total pressure, respectively. CH_3O_2 was generated in the chamber by photolysing one of two precursor gas mixtures. The first CH_3O_2 precursor system was a mixture of Cl_2 (Sigma Aldrich, ≥ 99.5 %) and CH_4 (BOC, CP grade, 99.5 %), where the Cl_2 was photolysed at ~365 nm (Phillips, TL-D36W/BLB, λ = 350–400 nm) to generate CH_3O_2 *via* the reactions:

$$Cl_2 + h\nu\ (365\ nm) \rightarrow Cl + Cl \quad (R6)$$

$$CH_4 + Cl \rightarrow CH_3 + HCl \quad (R7)$$

$$CH_3 + O_2 + M \rightarrow CH_3O_2 + M \quad (R1)$$

Typical reagent concentrations were $[CH_4]$ = 1.2–2.5 × 10^{16} molecule cm^{-3} and $[Cl_2]$ = 1.1–5.5 × 10^{15} molecule cm^{-3}. The second method used the photolysis of acetone (Sigma Aldrich, HPLC grade, ≥ 99.9 %) at 254 nm (GE G55T8/OH 7G) to produce CH_3O_2 *via* (R9) and (R10) followed by (R1):

$$(CH_3)_2CO + h\nu\ (254\ nm) \rightarrow 2CH_3 + CO \quad (R8)$$

$$(CH_3)_2CO + h\nu\ (254\ nm) \rightarrow CH_3 + CH_3CO \quad (R9)$$

Typical initial concentrations were $[(CH_3)_2CO]$ = 8.8 × 10^{14} molecule cm^{-3}. In the FAGE calibration experiments using the kinetic decays $[Cl_2]_0$ = 1.1 × 10^{14} molecule cm^{-3} with CH_4 at one of two concentrations: 2.5 × 10^{16} molecule cm^{-3} and 2.5 × 10^{17} molecule cm^{-3}. In the kinetic experiments performed to determine the absorption cross section of CH_3O_2 at 7487.98 cm^{-1}, $[Cl_2]_0$ = 1.1 × 10^{14} molecule cm^{-3} and $[CH_4]_0$ = 2.5 × 10^{16} molecule cm^{-3} at 80 mbar $He:O_2$ = 3:1 and $[Cl_2]_0$ = 1.0 × 10^{15} molecule cm^{-3} and $[CH_4]_0$ = 2.4 × 10^{16} molecule cm^{-3} at 100 mbar $N_2:O_2$ = 4:1.

2.2 FAGE instrument and calibration for CH_3O_2

The FAGE instrument in HIRAC has been described in detail previously (Winiberg et al., 2015; Onel et al., 2017a; Onel et al., 2017b). The instrument has a ~ 1 m long black anodised aluminium sampling tube with an inner diameter of 50 mm. The interior of the tube is held at a low pressure of 3.3 mbar and draws sample gas in through a 1 mm diameter pinhole mounted on one end of the tube at a rate of ~5 SLM. Two fluorescence cells are integrated into the tube, the centre of the first cell is

https://doi.org/10.5194/amt-2019-405
Preprint. Discussion started: 14 November 2019

Atmospheric Measurement Techniques Discussions

~300 mm from the pinhole, and the centre of the second cell is a further ~300 mm downstream, followed by a line of tubing that is connected to a rotary backed roots blower pump system (Leybold Trivac D40B and Ruvac WAU 251). The first cell is used to detect OH radicals but is not relevant to this work and is not discussed further, whereas the second cell is used for the CH_3O_2 measurements detailed here. High purity NO (BOC, N2.5 nitric oxide) is injected at 2.5 sccm using a mass flow controller (Brooks 5850S) into the centre of the gas flow ~25 mm prior to the second cell to convert CH_3O_2 radicals into CH_3O. Pulsed laser light at 297.79 nm is directed through the cell and propagates perpendicular to the gas flow and is used to excite the $A^2A_1(v_3' = 3) \leftarrow X^2E(v_3'' = 0)$ transition of CH_3O. The off resonant, red shifted fluorescence (320-430 nm) from CH_3O (A) is subsequently detected by a microchannel plate photomultiplier (Photek PMT325) using photon counting. Measurements are made at an excitation wavelength of 297.79 + 2.5 nm in order to determine the laser background, which is subtracted to leave only signal due to CH_3O fluorescence.

The FAGE technique is not absolute and therefore determination of the calibration factor, $C_{CH_3O_2}$, is required, to convert the measured signal $S_{CH_3O_2}$, to the CH_3O_2 concentration:

$$[CH_3O_2] = \frac{S_{CH_3O_2}}{C_{CH_3O_2}} \quad (1)$$

2.2.1 Calibration at atmospheric pressure - H_2O vapour photolysis in the presence of excess CH_4

This calibration procedure has been described in detail previously (Winiberg et al., 2015; Onel et al., 2017b), as such only important points are represented here. CH_3O_2 radicals were generated by photolysing water vapour in air (BOC, synthetic BTCA 178) at 184.9 nm to produce OH radicals, which then reacted with methane (BOC, CP grade, 99.5 %) to produce CH_3O_2:

$$H_2O + h\nu\ (185\ nm) \rightarrow OH + H \quad (R10)$$
$$OH + CH_4 \rightarrow CH_3 + H_2O \quad (R11)$$
$$CH_3 + O_2 + M \rightarrow CH_3O_2 + M \quad (R1)$$

The subsequent air/radical mixture was then sampled by the FAGE instrument. The concentration of CH_3O_2 generated is given by:

$$[CH_3O_2] = [OH] = [H_2O] \cdot \sigma \cdot \Phi \cdot F \cdot t \quad (2)$$

where σ is the absorption cross section of water vapour at 184.9 nm, (7.22 ± 0.22) × 10^{-20} cm^2 $molecule^{-1}$ (Cantrell et al., 1997; Creasey et al., 2000), Φ is the photo-dissociation quantum yield of OH at 184.9 nm (unity), t is the residence time of the gas in the photolysis field, which is ~16.6 and ~8.3 ms at 20 and 40 SLM respectively, and F is the lamp flux at 184.9 nm. The product $F \cdot t$ is determined using chemical actinometry (Winiberg et al., 2015). The 184.9 nm photon flux, F, is proportional to the electrical current supplied to the photolysis lamp and is varied to produce a range of CH_3O_2 radical concentrations. A typical calibration plot of the FAGE LIF signal vs. generated $[CH_3O_2]$ calculated using Eq. (2) is shown in the Supplementary Information (SI), Figure S1. An average of four calibrations gave $C_{CH_3O_2}$ = (8.03 ± 1.37) × 10^{-10} counts cm^3 $molecule^{-1}$ s^{-1} mW^{-1} where the error represents the overall uncertainty (17%) calculated using the statistical error (7%) and the systematic error (16%) at 1σ level (Onel et al., 2017b).

https://doi.org/10.5194/amt-2019-405
Preprint. Discussion started: 14 November 2019

Atmospheric Measurement Techniques Discussions

2.2.2 Calibration using kinetics of the CH_3O_2 temporal decay

The calibration described in the previous section is only valid when FAGE is sampling at atmospheric pressure. However, when sampling from lower pressures, as described in Sect. 2.1, the FAGE cell pressure decreases (0.9 mbar sampling from 100 mbar) and the calibration is no longer valid. An alternative calibration procedure using the kinetics of the CH_3O_2 self-reaction inside the HIRAC chamber allowed the FAGE instrument to be calibrated under the same conditions of pressure as the intercomparison experiments, including at lower pressures. Table 1 shows the sensitivity factors, $C_{CH_3O_2}$, obtained for each set of chamber conditions. Radicals were generated in the chamber in the same manner as those described in Sect. 2.1. However, instead of measuring steady state radical concentrations, the lamps were switched off and on at ~120 s intervals to produce a series of second–order decays, typically 4 per experiment, in which CH_3O_2 undergoes loss via self-reaction:

$$CH_3O_2 + CH_3O_2 \rightarrow CH_3OH + CH_2O + O_2 \quad \text{(R5a)}$$

$$CH_3O_2 + CH_3O_2 \rightarrow CH_3O + CH_3O + O_2 \quad \text{(R5b)}$$

Assuming no wall loss for CH_3O_2, the kinetic decays can be described by the integrated second order rate equation:

$$\frac{1}{[CH_3O_2]_t} = \frac{1}{[CH_3O_2]_0} + 2 \cdot k_{obs} \cdot t \quad (3)$$

where $[CH_3O_2]_t$ is the radical concentration at time t of the decay, $[CH_3O_2]_0$ is the initial concentration at the time, t_0, when the lamps are switched off, and k_{obs} is the observed rate coefficient. The observed rate coefficient is larger than the second–order rate coefficient of just the CH_3O_2 recombination reaction (R5) as the methoxy radicals generated by channel R5.b react rapidly with oxygen present in large excess to produce HO_2 (R3), which in turn reacts with CH_3O_2 (R12).

$$CH_3O + O_2 \rightarrow CH_2O + HO_2 \quad \text{(R3)}$$

$$CH_3O_2 + HO_2 \rightarrow 0.9CH_3OOH + 0.1CH_2O + 0.1H_2O + O_2 \quad \text{(R12)}$$

This further reaction of CH_3O_2 with HO_2 however does not stop the decay analysis, as in previous publications (Sander and Watson, 1980; Sander and Watson, 1981; McAdam et al., 1987; Kurylo and Wallington, 1987; Jenkin et al., 1988; Simon et al., 1990), being carried out with the assumption of second order kinetics. Modelling of the decay process with a variety of CH_3O_2 and HO_2 concentrations after the lamps were switched off and following the establishment of steady state conditions showed that Eq. (3) was valid within experimental error. With the rate constant for the bimolecular process R5 taken from the IUPAC as 3.5×10^{-13} molecule^{-1} cm^3 s^{-1} (Atkinson et al., 2006), a faster observed rate constant (defined by Eq. (3)) was obtained from the model with a value, 4.9×10^{-13} molecule^{-1} cm^3 s^{-1} consistent with that recommended by IUPAC, $(4.8 \pm 0.6) \times 10^{-13}$ molecule^{-1} cm^3 s^{-1} (1σ uncertainty; Atkinson et al., 2006). Substituting Eq. (1) into Eq. (3) allows the measured signal over the decay to be related to the instrument sensitivity by:

$$\frac{1}{(S_{CH_3O_2})_t} = \frac{1}{(S_{CH_3O_2})_0} + \frac{2 \cdot k_{obs} \cdot (t - t_0)}{C_{CH_3O_2}} \quad (4)$$

where $(S_{CH_3O_2})_t$ and $(S_{CH_3O_2})_0$ are the FAGE signal at time t and t_0 respectively. Taking the reciprocal of Eq. (4) gives:

$$(S_{CH_3O_2})_t = \left(\frac{1}{(S_{CH_3O_2})_0} + \frac{2 \cdot k_{obs} \cdot (t - t_0)}{C_{CH_3O_2}} \right)^{-1} \quad (5)$$

https://doi.org/10.5194/amt-2019-405
Preprint. Discussion started: 14 November 2019

Atmospheric Measurement Techniques Discussions

which is then used to fit to the experimental data with k_{obs} fixed to the value recommended by IUPAC for 298 K, 4.8×10^{-13} molecule^{-1} cm^3 s^{-1}. Figure 1 shows an example CH_3O_2 self-reaction decay trace obtained at 1000 mbar, where the red line shows the result of the fitting process.

However, as the HIRAC chamber is constructed from steel, the potential for a loss of CH_3O_2 to the walls was investigated. By incorporating the wall loss as a first-order process Eq. (5) becomes:

$$(S_{CH_3O_2})_t = \left(\left(\frac{1}{(S_{CH_3O_2})_0} + \frac{2 \cdot k_{obs}}{k_{loss} \cdot C_{CH_3O_2}} \right) \times \exp(k_{loss} \cdot (t - t_0)) - \left(\frac{2 \cdot k_{obs}}{k_{loss} \cdot C_{CH_3O_2}} \right) \right)^{-1} \quad (6)$$

Fitting Eqs. (5) and (6) to the experimental data is shown in Fig. 1. The extracted values for the sensitivity factor are the same for the fit without and with wall loss included: $C_{CH3O2} = (1.17 \pm 0.04) \times 10^{-9}$ counts cm^3 molecule^{-1} s^{-1} mW^{-1} (statistical errors at 1σ level). The close overlap of the fits without and with wall loss included and the negligible values extracted for k_{loss} fitting Eq. (6) demonstrates that wall losses are very small and can be neglected. This is evidenced further by the lack of an observable radical gradient across the chamber diameter as shown in Fig. S4 in the Supplementary Information.

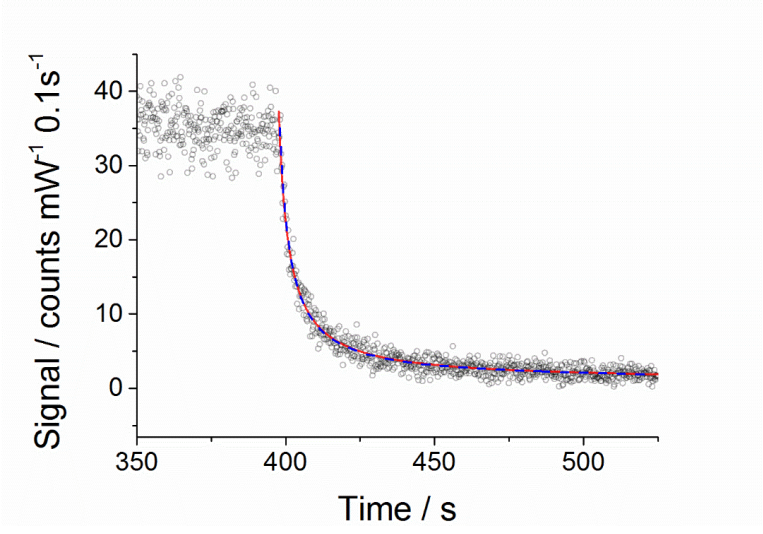

Figure 1. An example of a second-order decay of the FAGE CH_3O_2 signal (normalized for laser power fluctuations) with 0.1 second time resolution (black open circles) recorded at 295 K and a 1000 mbar air mixture. CH_3O_2 was generated using $[Cl_2] \sim 1.1 \times 10^{14}$ molecule cm^{-1} and $[CH_4] \sim 2.5 \times 10^{16}$ molecule cm^{-3}. At time zero (~400 s) the photolysis lamps were turned off to allow the radicals to decay. Fitting of Eq. (5) to the data (red line) gave $C_{CH3O2} = (1.18 \pm 0.02) \times 10^{-10}$ counts cm^3 molecule^{-1} s^{-1} mW^{-1}. A fit including the wall loss rate, k_{loss} (Eq. (6), see text) is shown by the blue dashed line and gave $C_{CH3O2} = (1.15 \pm 0.03) \times 10^{-10}$ counts cm^3 molecule^{-1} s^{-1} mW^{-1}. The close overlap of the two fits shows the wall loss is insignificant and may be ignored. The C_{CH3O2} errors given above represent statistical uncertainties at 1σ level.

https://doi.org/10.5194/amt-2019-405
Preprint. Discussion started: 14 November 2019

Atmospheric Measurement Techniques Discussions

Table 1. Average sensitivity factors for the FAGE instrument using the CH_3O_2 kinetic decay method under each chamber environment. Examples of these decays can be found in Figure 1 above and in the SI, Figures S2 and S3, and reported values are typically from an average of 8 decays. All the data were fitted using Eq. (5). The errors given in the table are overall uncertainties (13%) at 1σ level.

Chamber Conditions	$C_{CH_3O_2}$ / counts cm^3 molecule^{-1} s^{-1} mW^{-1}
80 mbar, He + O_2	(3.83 ± 0.50) × 10^{-9}
100 mbar, Air	(2.80 ± 0.37) × 10^{-9}
1000 mbar, Air	(1.16 ± 0.15) × 10^{-9}

Table 1 shows the average sensitivity factors obtained fitting Eq. (5) to a typical number of 8 temporal decays of $S_{CH_3O_2}$ under each of the chamber conditions, and example decay traces for the 80 and 100 mbar experiments can be found in the SI, Figs S2 and S3 respectively. These factors are used for their respective experimental conditions. For the 1000 mbar intercomparison experiments with CRDS, an average of the water vapour photolysis sensitivity factor at 1000 mbar, $C_{CH3O2,\ H2O}$ = (8.03 ± 1.37) × 10^{-10} counts cm^3 molecule^{-1} s^{-1} mW^{-1}, and the average sensitivity factor obtained from the kinetic decay, $C_{CH3O2,\ kinetic}$ = (1.16 ± 0.15) × 10^{-9} counts cm^3 molecule^{-1} s^{-1} mW^{-1} (Table 1), is used, giving $C_{CH3O2,\ av.}$ = (9.81 ± 2.03) × 10^{-10} counts cm^3 molecule^{-1} s^{-1} mW^{-1}. We make a brief comment regarding the difference in the sensitivity factors $C_{CH3O2,\ H2O}$ and $C_{CH3O2,\ kinetic}$, for which the ratio is ~ 0.7, showing a ~30% difference, although the two calibration methods have overlapping error limits at 2σ level. The kinetic method relies on the rate coefficient k_{obs} for the CH_3O_2 self-reaction as recommended by IUPAC (Atkinson et al., 2006), which has a quoted 2σ uncertainty of 23%. In a separate paper we will present a detailed study of the kinetics of the CH_3O_2 self-reaction, and its temperature dependence, and report a revised rate coefficient for this reaction at 298 K.

2.2.3 FAGE measurements of CH_3O_2 concentration gradient across the HIRAC diameter

Measurement of radical gradients across the chamber diameter have been performed previously for HO_2 radicals (Onel et al., 2017a), where no gradient was observed until measuring <10 cm from the chamber wall where the signal began to decrease, ultimately by ~16 % at the point at which the FAGE sampling pinhole was level with the chamber walls. To investigate any similar gradient effects for CH_3O_2, a steady state concentration of CH_3O_2 was generated in the chamber at atmospheric pressure by photolysing O_3 in the presence of air and methane:

$$O_3 + h\nu\ (254\ nm) \rightarrow O_2 + O(^1D) \quad (R12)$$

$$O(^1D) + CH_4 \rightarrow CH_3 + OH \quad (R13)$$

$$CH_3 + O_2 + M \rightarrow CH_3O_2 + M \quad (R1)$$

Ozone and methane were present in the chamber at ~2.5 × 10^{13} molecule cm^{-3} and 2.5 × 10^{17} molecule cm^{-3} respectively. The FAGE inlet was translated across the width of the chamber and the CH_3O_2 signal was observed to show no decrease within the ~10% 1σ statistical error of each measurement up until the point at which the pinhole was level with the chamber walls. Moving the instrument further backwards positioned the pinhole inside the ISO-K160 coupling flange and effectively ~4 cm behind the chamber walls where there is likely to be little air movement. This position is analogous to that of the CRDS mirrors, which are recessed into the chamber walls as they mount to the outside of the chamber (see Sect. 2.3). In this position a signal

https://doi.org/10.5194/amt-2019-405
Preprint. Discussion started: 14 November 2019

Atmospheric Measurement Techniques Discussions

drop of ~14 % was observed, within the statistical error margins of the measurements. A plot of the radical gradient is shown in the Supplementary Information, Figure S4.

2.3 CRDS set-up

The optical path of the CRDS spectrometer within the HIRAC chamber is shown in Fig. 2 and is the same spectrometer as used to probe HO_2 across the chamber's diameter, and which has been described previously (Onel et al., 2017a).

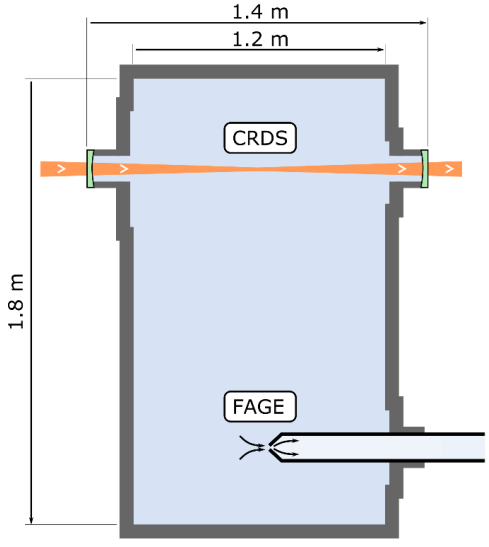

Figure 2. Longitudinal (horizontal) section of the HIRAC chamber. The CRDS spectrometer probes the CH_3O_2 concentration as an average across the chamber's diameter, while the FAGE instrument probes CH_3O_2 in the chamber at a single point close to the centre.

The cavity is formed by two highly reflective 1 in. diameter mirrors (99.999 %, Layertec, curvature radius = 1 m) housed in custom built mounts that allow the mirrors to be tilted slightly whilst maintaining a gas-tight seal. The position of the mirror on the laser injection side is modulated along the cavity axis by a few microns using a piezoelectric transducer at ~10 Hz, with the overall distance between the two mirrors being ~1.4 m. Laser light of ~1.335 μm is generated by a distributed feedback (DFB) fibre pig-tailed diode laser (NTT Electronics, NLK1B5EAAA) held in a butterfly laser diode mount (Thorlabs LM14S2). The electrical current that drives the laser diode and thermoelectric cooler is generated by a Thorlabs ITC502 driver. The DFB is connected to an inline optical isolator (Thorlabs IO-H-1335APC), an acousto-optic modulator (AOM, Gooch & Housego Fibre-Q M040-0.5C8H-3-F2S) and a fibre collimator (Thorlabs CFC-8X-C). The laser light is then guided into the cavity by two silver mirrors (Thorlabs PF10-03-P01). On the detection side of the cavity, light leaking out of the mirror is directed onto another silver mirror that guides the light through a f = 30 mm focusing lens (Thorlabs LA1805-C) onto an InGaAs photodiode (Thorlabs DET10C/M) that is isolated from ambient light by a 1250 nm longpass filter (Thorlabs FELH1250). The photodiode signal is amplified (FEMTO DLPCA-200) and sent to a data acquisition unit (DAQ, National Instruments USB-6361) and to a custom-built comparator that acts as a trigger unit. The comparator compares the amplified photodiode signal with a manually adjustable threshold voltage, and upon reaching a preset threshold the AOM is switched off, stopping the injection of light into the cavity within tens of nanoseconds and initiating a ring-down event. The DAQ is simultaneously triggered and acquires the signal ring-down. The system resets after a set time (typically 5 ms) ready for the

https://doi.org/10.5194/amt-2019-405
Preprint. Discussion started: 14 November 2019

Atmospheric Measurement Techniques Discussions

next event. The acquired data are processed using a custom made LabView program that fits the ring-down events with an exponential function to extract the ring-down time, τ. The ring-down time can then be converted into the absorption coefficient, α:

$$\alpha = \frac{1}{c} \times (1/\tau - 1/\tau_0) \quad (7)$$

where τ and τ_0 are the ring-down time with and without CH_3O_2 radicals present, respectively, and c is the speed of light. τ_0 would be obtained in a typical experiment by recording ring-down events for ~ 1 minute before switching on the photolysis lamps in the chamber. As it is not possible to measure τ_0 and τ simultaneously, the background was monitored regularly during each experiment by switching off the photolysis lamps and allowing the signal to return to the baseline.

The CH_3O_2 absorption feature used in these measurements is a band associated with the $A^2A' \leftarrow X^2A''$ electronic transition centred around 7488 cm^{-1}, and has been documented in previous work (Faragó et al., 2013, Atkinson and Spillman, 2002, Pushkarsky et al., 2000). There are interfering methane and water vapour lines in this region, and these together with the change in [CH_3O_2] during longer ($\gtrsim$ 5 min) scanning times did not allow us to generate a continuous, high resolution scan across the CH_3O_2 transition. Instead, as shown in Fig. 3, the absorption spectrum was mapped out as a series of point measurements at fixed wavelengths, normalised by the absorption at the optimum measurement point, 7487.98 cm^{-1} (rounded to 7488 cm^{-1} henceforth), where the absorption feature is sufficiently strong and furthest in wavelength from interfering methane absorption lines and where the CH_3O_2 cross section was determined (Sect. 3.2). Each data point in Fig. 3 was obtained by measuring the absorption coefficient, $\alpha_{7488\ cm^{-1}}$, and the baseline (lamps on, then off) at 7488 cm^{-1} followed by measuring α_{CH3O2} and baseline at another wavelength on the absorption feature and then reverting to measuring at 7488 cm^{-1} again. This pattern was repeated multiple times for different wavelengths to build up an absorption feature, with all data points normalised to $\alpha_{7488\ cm^{-1}}$ and then multiplied by the CH_3O_2 cross section at 7488 cm^{-1} (Sect. 3.2) to obtain the absorption spectrum shown in Fig. 3. The method was used to measure the CH_3O_2 absorption spectrum under each of the three experimental conditions detailed in Sect. 2.1: 80 mbar (He + O_2) and 100 mbar and 1000 mbar of synthetic air.

3 Results

3.1 CH_3O_2 absorption spectrum and comparison with the literature

Figure 3 shows that the relatively broad absorption feature obtained in this work in the range from ~7486 to 7491 cm^{-1} is almost the same at 80 mbar He:O_2 = 3:1 and at 100 and 1000 mbar of synthetic air. As shown in Fig. 3, the spectrum found in this work agrees well with the general shape of the CH_3O_2 spectrum measured by Faragó et al. (2013) at 67 mbar He:O_2 ~ 1:1 but scaled to reflect the very recent update to the absolute absorption cross-section reported by Fittschen (2019) which gave $\sigma_{7489\ cm^{-1}} = 2.2 \times 10^{-20}$ cm^2 $molecule^{-1}$. The peaks at the top of the spectral feature reported by Faragó et al. (2013) are not reproduced in this work owing to the method of generating the spectrum, which did not allow for a high resolution (Sect. 2.3), and a potential small difference in wavelength compared to λ in the spectrum reported by Faragó et al. (2013). Previously Pushkarsky et al. (2000) measured the CH_3O_2 absorption spectrum over a larger wavenumber range (7300–7700 cm^{-1}) where the ν_{12} transition is located at 7488 cm^{-1} in agreement with this work. In addition, if the CH_3O_2 spectrum at 27 mbar N_2:O_2 = 4:1 reported by Atkinson and Spillman (2002) were shifted by ~2 cm^{-1} toward higher wavenumbers compared to this work and the study of Faragó et al. (2013), the shape of the ν_{12} band from Atkinson and Spillman is in agreement with the results shown in Fig. 3.

The similarity of the results at 80 mbar He:O_2 = 3:1 and at 100 and 1000 mbar of air reported in this work and their agreement with the previous measurements performed at relatively low pressures (Fittschen, 2019; Faragó et al., 2013;

https://doi.org/10.5194/amt-2019-405
Preprint. Discussion started: 14 November 2019

Atmospheric Measurement Techniques Discussions

Atkinson and Spillman, 2002; Pushkarsky et al., 2000) can be explained by an overlap of several individual absorption lines resulting in a spectral structure in the range from ~7486 to 7491 cm^{-1} with practically no pressure dependence observed between ~30–1000 mbar. Therefore, it can be assumed that the absorption cross section at 7488 cm^{-1}, σ(7488 cm^{-1}), is the same under the conditions used in this work, i.e. at 80 mbar of He and O_2 and at 100 and 1000 mbar of air.

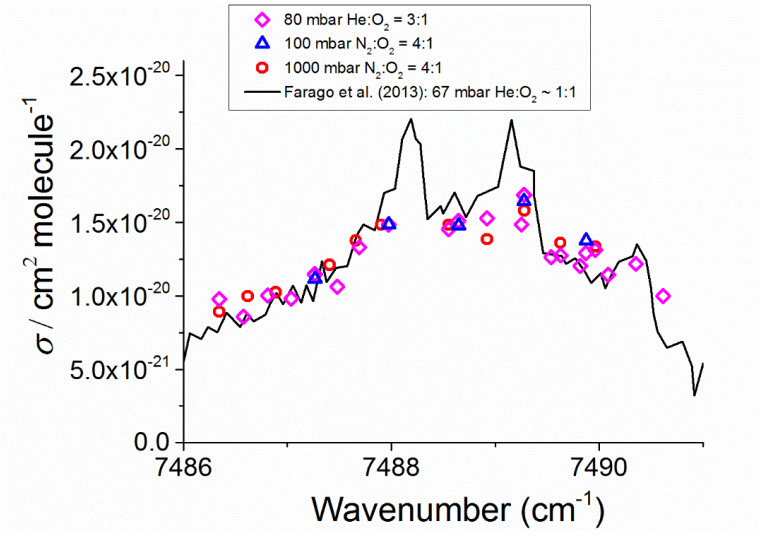

Figure 3. CH_3O_2 absorption spectrum at 295 K. The measured absorption spectrum scaled to the absolute cross section determined at 7488 cm^{-1} using the kinetics of the CH_3O_2 decay monitored using CRDS (Sect. 3.2 below). The black line represents the CH_3O_2 spectrum measured by Faragó et al. (2013) at 67 mbar He:O_2 ~ 1:1 but with the absolute cross-section scaled to reflect the recent update reported by Fittschen (2019) giving $\sigma_{7489\ cm^{-1}} = 2.2 \times 10^{-20}$ cm^2 $molecule^{-1}$.

3.2 Determination of the absorption cross section of CH_3O_2 at 7488 cm^{-1}

The kinetics of the CH_3O_2 temporal decay by its self-reaction (Reaction R5) were used to determine the absorption cross section of CH_3O_2 at 7488 cm^{-1}, σ(7488 cm^{-1}). CH_3O_2 radicals were generated by using CH_4/Cl_2/synthetic air mixtures (Sect. 2.1) with the chamber UV lamps switched on to generate Cl atoms (R6). By extinguishing the UV lamps, CH_3O_2 radicals were removed by self-reaction and wall loss. Figure 4 shows an example of a kinetic decay obtained at 100 mbar N_2:O_2 = 4:1 using CRDS. The experimental data were fitted by using two functions described by Eqs. (8) and (9), which are closely related to Eqs. (4) and (5) used in the analysis of the CH_3O_2 decays measured using FAGE. Equation (8) assumes that the wall loss of CH_3O_2 is negligible and hence the removal of CH_3O_2 can be described by the integrated second–order rate law equation, leading to:

$$\alpha_t = \left(\frac{1}{\alpha_0} + \frac{2 \cdot k_{obs.}(t - t_0)}{\sigma(7488\ cm^{-1})}\right)^{-1}, \quad (8)$$

where α_t is the CH_3O_2 absorption coefficient at 7488 cm^{-1} and at time t, α_0 is the absorption coefficient at time zero of the reaction when the lamps are switched off, t_0, and k_{obs} is the observed rate coefficient of the self-reaction at 298 K, k_{obs} = (4.8 ± 0.6) × 10^{-13} cm^3 $molecule^{-1}$ s^{-1} (Atkinson et al., 2006).

For completeness, Equation (9) includes the CH_3O_2 wall loss as a first-order process, leading to:

https://doi.org/10.5194/amt-2019-405
Preprint. Discussion started: 14 November 2019

Atmospheric Measurement Techniques Discussions

$$\alpha_t = \left(\left(\frac{1}{\alpha_0} + \frac{2 \cdot k_{obs.}}{k_{loss} \cdot \sigma(7488\ cm^{-1})} \right) \times \exp(k_{loss}(t - t_0)) - \left(\frac{2 \cdot k_{obs.}}{k_{loss} \cdot \sigma(7488\ cm^{-1})} \right) \right)^{-1}, \quad (9)$$

where k_{loss} is the rate coefficient describing the CH_3O_2 wall loss (Onel et al., 2017a).

Figure 4 shows that the fits given by Eqs. (8) and (9) to the data overlap over all of the temporal CH_3O_2 decay and the values of σ(7488 cm^{-1}) extracted by the two fits are in a very good agreement: (1.47 ± 0.07) × 10^{-20} cm^2 molecule^{-1} (Eq. (8)) and (1.50 ± 0.07) × 10^{-20} cm^2 molecule^{-1} (Eq. (9)), where the quoted errors are statistical uncertainties. From fitting Eq. (8) to the temporal decays obtained at 100 mbar of synthetic air, an averaged value of (1.51 ± 0.19) × 10^{-20} cm^2 molecule^{-1} was obtained, where the error represents 1σ overall uncertainty (13%). Fitting Eq. (8) to the data at 80 mbar He:O_2 = 3:1 (Fig. S5), gave an average value of σ(7488 cm^{-1}) = (1.46 ± 0.17) × 10^{-20} cm^2 molecule^{-1} (1σ overall uncertainty), in very good agreement with the value at 100 mbar of air. The average of the results at 80 mbar He:O_2 = 3:1 and 100 mbar of air, 1.49 × 10^{-20} cm^2 molecule^{-1}, is in excellent agreement with the determination of Atkinson and Spillman (2002): $\sigma_{max}(\nu_{12})$ = (1.5 ± 0.8) × 10^{-20} cm^2 molecule^{-1} and consistent with the estimation of ~1.0 × 10^{-20} cm^2 molecule^{-1} for $\sigma_{max}(\nu_{12})$ obtained using the CH_3O_2 spectrum reported by Pushkarsky et al. (2000). To enable a comparison at 7487.98 cm^{-1} with the very recent measurement of Fittschen (2019), who found 2.20 × 10^{-20} cm^2 molecule^{-1} at 7489.16 cm^{-1}, σ(7487.98 cm^{-1}) = 1.49 × 10^{-20} cm^2 molecule^{-1} obtained in this work was multiplied by the σ(7489.16 cm^{-1}):σ(7487.98 cm^{-1}) ratio obtained by using the high resolution spectrum reported by Faragó et al. (2013) (Fig. 3). The obtained value, σ(7489.16 cm^{-1}) = (1.9 ± 0.3) × 10^{-20} cm^2 molecule^{-1} is in reasonable agreement with the result of Fittschen (2019), σ(7489.16 cm^{-1}) = 2.2 × 10^{-20} cm^2 molecule^{-1}.

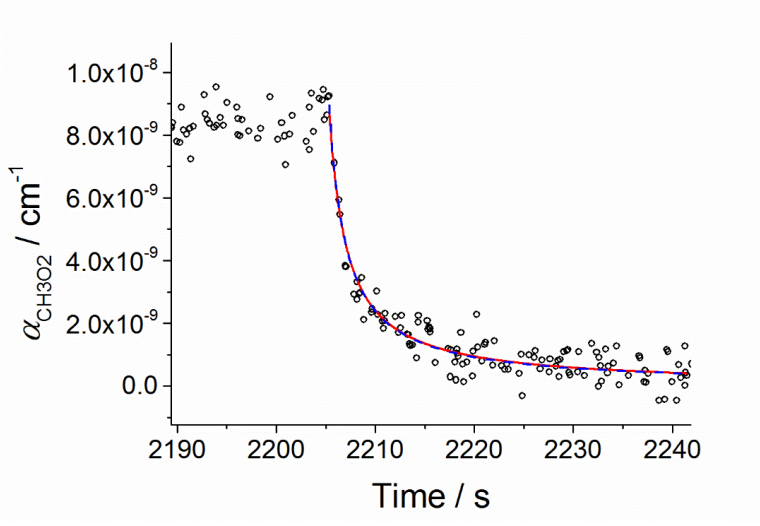

Figure 4. Second-order decay of the CH_3O_2 absorption coefficient at 7488 cm^{-1} monitored by CRDS. Experiment carried out at 295 K and 100 mbar of synthetic air; $[CH_4]_0$ = 2.4 × 10^{16} molecule cm^{-3} and $[Cl_2]_0$ = 1.0 × 10^{15} molecule cm^{-3}. At time 2205 s the photolysis lamps were turned off (time t_0). Fitting Eq. (8) to the data (red line) gave σ(7488 cm^{-1}) = (1.47 ± 0.07) × 10^{-20} cm^2 molecule^{-1}. A fit including the wall loss rate, k_{loss} (Eq. (9)) is shown by the blue dashed line and resulted in σ(7488 cm^{-1}) = (1.50 ± 0.07) × 10^{-20} cm^2 molecule^{-1}. The error limits are statistical errors at 1σ level.

3.3 Determination of the CRDS limit of detection

The CRDS limit of detection (*LOD*) has been computed using Allan-Werle deviation plots (Werle et al., 1993; Onel et al., 2017a) obtained by continuously recording single ring-down events for 1–2 h after delivering either acetone or methane in

https://doi.org/10.5194/amt-2019-405
Preprint. Discussion started: 14 November 2019

Atmospheric Measurement Techniques Discussions

typical concentrations to the chamber filled with the bath gas (He:O_2 = 3:1 at 80 mbar and synthetic air at 100 and 1000 mbar, respectively). The Allan-Werle deviation, $\sigma_A(n)$, is $(1/\sqrt{2})$ times the root-mean-square value of the difference between adjacent points and gives an estimate of the error, $\delta\alpha$, between successively measured absorption coefficients for a given averaging size n. For a signal-to-noise ratio (S/N) of 2, the limit of detection for CH_3O_2 was determined as LOD_{CH3O2} = $(2\delta\alpha_{min})/\sigma_{CH3O2}$, where σ_{CH3O2} = 1.49 × 10^{-20} cm^2 $molecule^{-1}$ is the CH_3O_2 cross section at 7488 cm^{-1}, and is shown in Table 2. The optimum CRDS sensitivity under all conditions is achieved averaging ~500 ring-down events, requiring ~77 s at an acquisition rate of 6.5 Hz on average, with an example shown in Fig. 5.

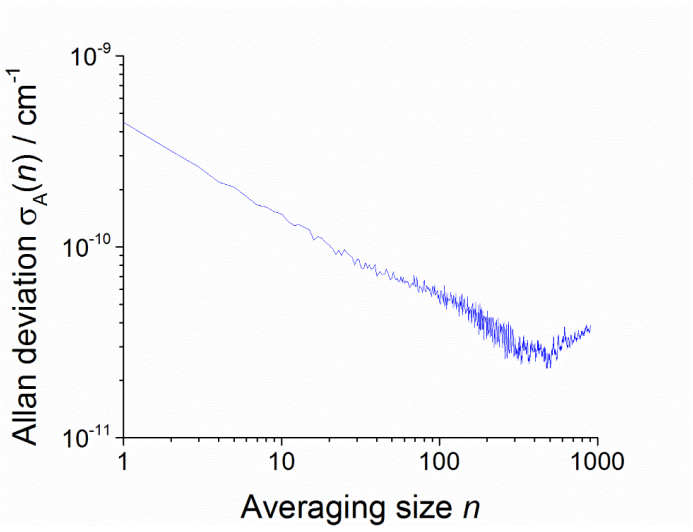

Figure 5. An example of the Allan-Werle deviation plot of the absorption coefficient at 7488 cm^{-1} in the absence of CH_3O_2 and the presence of a typical acetone concentration of 8.8 × 10^{14} molecule cm^{-3} at 1000 mbar against the number of ring-down events averaged, n. For S/N = 2 the minimum detectable absorption coefficient for a single ring-down measurement is 4.5 × 10^{-10} cm^{-1}, which decreases to a minimum of 2.89 × 10^{-11} cm^{-1} after n = 500 (requiring 77 s at an acquisition rate of 6.5 Hz).

As the filter (FELH1250 Thorlabs, cut-off wavelength: 1250 nm) used to cut-off the laboratory visible light from the background of the CRDS measurements allowed some of the 254 nm light generated by the HIRAC lamps to be transmitted and then detected by the InGaAS photodiode detector, the CRDS sensitivity was worse in the experiments using acetone/O_2/254 nm lamps as a source of CH_3O_2 compared to the experiments using Cl_2/CH_4/O_2/UV black lamps to generate CH_3O_2. Therefore, separate Allan-Werle deviation plots were constructed using measurements of single ring-down events after filling HIRAC with the bath gas and turning the 254 nm lamps on. Then, the composite error, calculated as the sum in quadrature of $\delta\alpha$ obtained in the presence of acetone and $\delta\alpha$ determined in the absence of acetone but keeping the 254 nm lamps turned on, was used to determine the LOD of CRDS in the acetone/O_2/254 nm experiments (Table 2). The composite LOD(acetone/O_2/254 nm lamps) was on average ~55% greater than the LOD determined with the UV lamps off and in the absence of acetone, LOD(bath gas); and on average LOD(Cl_2/CH_4/O_2/UV black lamps) was ~40% higher than LOD(bath gas)

https://doi.org/10.5194/amt-2019-405
Preprint. Discussion started: 14 November 2019

Atmospheric Measurement Techniques Discussions

Table 2. CRDS detection limits for CH_3O_2 calculated at 80 mbar $He:O_2$ = 3:1 and 100 mbar and 1000 mbar of synthetic air for single ring-down measurements (Δt = 0.15 s), the optimum averaging time obtained from Allan-Werle deviation plot, $\Delta t_{opt.}$ (77 s under all experimental conditions) and Δt = 60 s.

Bath gas	p_{HIRAC} / mbar	Reagent delivered to HIRAC	LOD_{CH3O2} / 10^9 molecule cm^{-3}		
			Δt = 0.15 s	Δt = 60 s	Δt_{opt} = 77 s.
$He:O_2$ = 3:1	80	acetone[a]	120	7.5	6.4
Air	100	acetone[a]	133	8.6	6.8
		methane[b]	78	6.0	5.4
Air	1000	acetone[a]	147	7.3	6.1

[a] using the composite error calculated as the sum in quadrature of $\delta\alpha$ obtained using a typical concentration of acetone, 8.8 × 10^{14} molecule cm^{-3}, and $\delta\alpha$ determined in the absence of acetone but keeping the 254 nm lamps turned on during all measurement.
[b] $[CH_4]$ = 2.4 × 10^{16} molecule cm^{-3}.

As the daytime concentrations of CH_3O_2 have been calculated using an atmospheric box-model to peak at ~10^7–10^8 molecule cm^{-3} (Whalley et al., 2010; Whalley et al., 2011; Whalley et al., 2018), the current CRDS sensitivity is insufficient for the detection of ambient $[CH_3O_2]$. The typical concentrations of CH_4 and acetone in ambient air are orders of magnitude lower than $[CH_4]$ and $[(CH_3)_2CO]$ used in the HIRAC experiments. However, water vapour, which is present in the atmosphere in much larger concentrations (typically ~10^{17} molecule cm^{-3}) than in HIRAC for these experiments (~ 10^{13} – 10^{14} molecule cm^{-3}), will significantly absorb in this wavelength region and contribute towards the background of the measurements. The limits of detection shown in Table 2 allow for HIRAC measurements of $[CH_3O_2] \gtrsim 10^{10}$ molecule cm^{-3} in steady-state (where averaging times of ~60 s can be used) under all conditions used, and kinetic measurements of $[CH_3O_2] \gtrsim 10^{11}$ molecule cm^{-3} with the present instrument resolution time (0.15 s) at 80 mbar $He:O_2$ = 3:1 and 100 mbar of air.

The CRDS sensitivity could be further improved by increasing the frequency of the ring–down events and using a cavity length above the current 1.4 m length. Although the origin band centred at 7388 cm^{-1} is about three times stronger than the methyl torsional band at 7488 cm^{-1} (Pushkarsky et al., 2000; Chung et al., 2007), the latter was targeted because absorption due to water vapour is between one and three orders of magnitude weaker there (assuming 1% v/v, atmospheric pressure) (Gordon et al., 2017).

3.4 Intercomparison of CRDS and FAGE CH_3O_2 measurements

All the intercomparison measurements have been performed at 7488 cm^{-1}, where the CH_3O_2 cross section was determined using CRDS (Sect. 3.2). For the measurements at 80 mbar $He:O_2$ (3:1) and 100 mbar $N_2:O_2$ (4:1), CH_3O_2 was generated either from the photolysis of acetone at 254 nm in the presence of O_2 or from the photolysis of Cl_2 using UV black lamps in the presence of CH_4/O_2. At 1000 mbar of synthetic air, the overlap of the methane absorption lines due to the pressure broadening resulted in a significant CH_4 absorption over the range from 7486–7491 cm^{-1} in the background of the CH_3O_2 measurements. Therefore, all the measurements at 1000 mbar have been carried out using the photolysis of acetone/O_2 at 254 nm. The data recorded by CRDS using acetone/O_2 were more scattered than the CRDS data recorded using $Cl_2/CH_4/O_2$ for the reasons discussed above (see Figs. 6a and 8a in comparison with Fig. 7a) and were the main contributors to the scatter on $[CH_3O_2]_{CRDS}$ in the correlation plots (Figs. 6b, 7b and 8b below). There was less signal noise present in the FAGE measurements, where the most significant source of noise is the shot noise (Poisson noise), which increases with the number of photons counted by the detector (Figs. 1, S2 and S3) and results in a scatter on the FAGE data growing with $[CH_3O_2]$ in Figs 6a, 7a and 8a.

https://doi.org/10.5194/amt-2019-405
Preprint. Discussion started: 14 November 2019

Atmospheric Measurement Techniques Discussions

CH_3O_2 was generated over a range of concentrations, 2–26 × 10^{10} molecule cm^{-3} at 80 mbar of He + O_2 mixture, 2–60 × 10^{10} molecule cm^{-3} at 100 mbar of synthetic air and 2–30 × 10^{10} molecule cm^{-3} at 1000 mbar of synthetic air. The comparison involved both periods with lamps on where the concentration of CH_3O_2 was changing slowly, and where the lamps were turned off and the rapid decay of CH_3O_2 was observed. Figures 6a, 7a and 8a show examples of time-resolved CH_3O_2 concentrations where the lamps were turned on and off. CRDS absorption coefficients were converted into concentrations using the absorption cross section determined by studying the second-order recombination kinetics, σ(7488 cm^{-1}) = (1.49 ± 0.19) × 10^{-20} cm^2 $molecule^{-1}$ (Sect. 3.2). The FAGE signals were converted into [CH_3O_2] using the sensitivity factor derived from the analysis of the temporal decays of CH_3O_2 at 80 mbar of He + O_2 mixture and 100 mbar of air, (3.83 ± 0.50) × 10^{-9} counts cm^3 $molecule^{-1}$ s^{-1} mW^{-1} and (2.80 ± 0.37) × 10^{-9} counts cm^3 $molecule^{-1}$ s^{-1} mW^{-1}, respectively. The gradient of the correlation plot of the CH_3O_2 concentrations determined by FAGE (*y*-axis) and CRDS (*x*-axis) at 80 mbar of He + O_2 (Fig. 6b) is 1.03 ± 0.05, showing an overall level of agreement within 3%. The gradient of the correlation plot of the CH_3O_2 concentrations determined by FAGE (*y*-axis) and CRDS (*x*-axis) at 100 mbar of air (Fig. 7b) is 0.95 ± 0.02, showing an overall level of agreement within 5%.

At 1000 mbar of air, the FAGE signal observed in HIRAC could be calibrated in one of two ways, either via the photolysis of water vapour to generate OH followed by reaction with CH_4 to form CH_3O_2, or via the kinetic analysis of second order temporal decays of CH_3O_2. The conversion of the FAGE signals into [CH_3O_2] at 1000 mbar air for the intercomparison with CRDS shown in Figs. 8a and 8b was based on the average of the results of the water vapour calibration method and the kinetic decay calibration method, which gives $\overline{C}_{CH_3O_2}$ = (9.81 ± 2.03) × 10^{-10} counts cm^3 $molecule^{-1}$ s^{-1} mW^{-1} (Sect. 2.2.2)). The gradient of the overall correlation plot (Fig. 8b) using $\overline{C}_{CH_3O_2}$ is 1.09 ± 0.06, showing agreement to within 9%. Figure S6 in the Supplementary Information shows separately the two correlation plots obtained using the sensitivities from the two methods of calibration for FAGE: $C_{CH_3O_2}$ = (8.03 ± 1.37) × 10^{-10} counts cm^3 $molecule^{-1}$ s^{-1} mW^{-1} (water vapour calibration method) and $C_{CH_3O_2}$ = (1.16 ± 0.15) × 10^{-9} counts cm^3 $molecule^{-1}$ s^{-1} mW^{-1} (second order kinetic decay method). The gradients of the two linear fits are: 1.35 ± 0.07 (water vapour calibration) and 0.92 ± 0.05 (kinetic method of calibration). Therefore, a significantly better agreement (within 8%) was obtained by using the kinetic method for the calibration of FAGE compared with using the water vapour method for calibration of FAGE (35% agreement). Better agreement is expected when using the kinetic method to calibrate FAGE, as this is the same method used to determine the absorption cross section and hence calibrate of the CRDS method, and the intercomparison is not subject to any error in the rate coefficient, k_{obs} for the CH_3O_2 self-reaction. We consider that the main contribution to the discrepancy in C_{CH3O2} values obtained by the two methods of calibration derives from an overestimation of the reported value of the observed rate coefficient for the CH_3O_2 self-reaction, k_{obs} = (4.8 ± 0.6) × 10^{-13} $molecule^{-1}$ cm^3 s^{-1} (1σ error) at 298 K (Atkinson et al., 2006). In a subsequent paper we will report a revised k_{obs}, which will bring into agreement the two methods of calibration.

https://doi.org/10.5194/amt-2019-405
Preprint. Discussion started: 14 November 2019

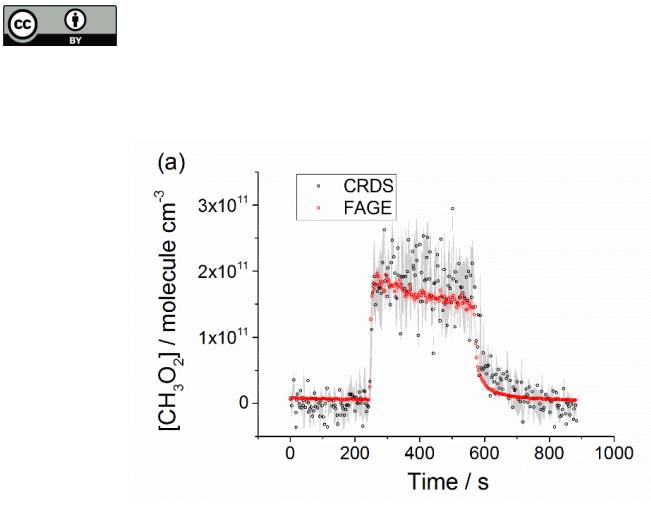

Figure 6. (a) Comparison of CH_3O_2 measurement at 80 mbar He:O_2 (3:1) where the lamps were turned on at t ~ 250 s for ~ 5 min to generate CH_3O_2 and then turned off again. The measurement by FAGE is shown in red and the measurement by CRDS is plotted in black. CH_3O_2 radicals were generated using the 254 nm photolysis of $(CH_3)_2CO$ (8.8×10^{14} molecule cm^{-3}). The 1σ statistical errors generated by the data averaging are shown as grey (CRDS) and red (FAGE) shadows. (b) Correlation plot at 80 mbar He:O_2 (3:1) combining the data obtained using acetone/O_2/254 nm lamps with the data generated using Cl_2/CH_4/O_2/UV black lamps. $[CH_3O_2]$ measured by FAGE is plotted against $[CH_3O_2]$ measured by CRDS. The linear fit to the data generates a gradient of 1.03 ± 0.05 and an intercept of (-1.7 ± 0.5) × 10^{10} molecule cm^{-3}. The linear fits were generated using the orthogonal distance regression algorithm; fit errors at 2σ level. In both panels $[CH_3O_2]_{FAGE}$ was determined using a calibration factor of 3.83×10^{-9} counts cm^3 molecule^{-1} s^{-1} mW^{-1} and $[CH_3O_2]_{CRDS}$ was calculated using a cross section of 1.49×10^{-20} cm^2 molecule^{-1}. Each point is an averaged value over 3 s.

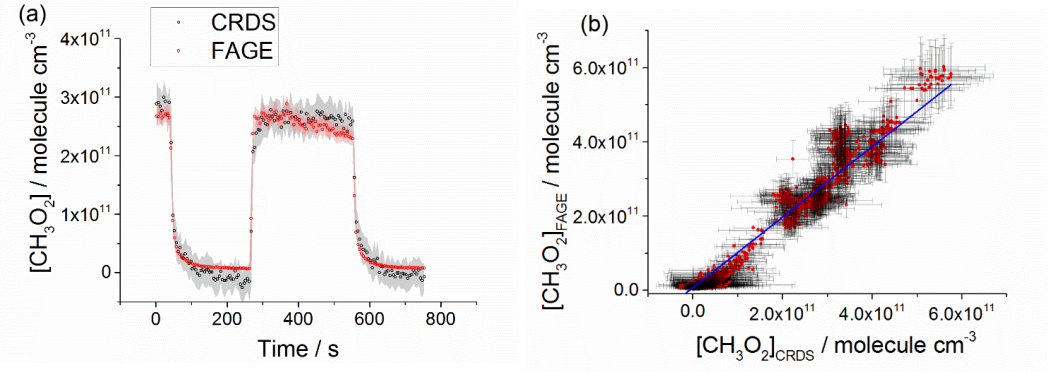

Figure 7. Comparison of CH_3O_2 measurement (a) and the correlation plot at 100 mbar N_2:O_2 (4:1) (b). In both figures $[CH_3O_2]_{FAGE}$ was computed using a calibration factor of 2.80×10^{-9} counts cm^3 molecule^{-1} s^{-1} mW^{-1} and $[CH_3O_2]_{CRDS}$ was determined using a cross section of 1.49×10^{-20} cm^2 molecule^{-1}. Each point is an averaged value over 5 s. Figure (a) shows the measurement by FAGE (red) and the measurement by CRDS (black) where the CH_3O_2 radicals were generated by the photolysis of Cl_2 (2.5×10^{15} molecule cm^{-3}) in the presence of CH_4 (2.4×10^{16} molecule cm^{-3}) and O_2. The UV black lamps were alternately switched on and off: the lamps were turned off at t ~ 40 s and then turned on at t ~ 250 s for ~ 5 min before being switched off again. The 1σ statistical errors generated by the data averaging are shown as grey (CRDS) and red (FAGE) shadows. Figure (b) combines the data obtained using acetone/O_2/254 nm lamps with the data generated using Cl_2/CH_4/O_2/UV black lamps. $[CH_3O_2]$ measured by FAGE is plotted versus $[CH_3O_2]$ measured by CRDS. The linear fit to the data is obtained using the orthogonal distance regression algorithm and results in a gradient of 0.95 ± 0.02 and an intercept of (7.0 ± 0.4) × 10^9 molecule cm^{-3}; fit errors given at 2σ level.

https://doi.org/10.5194/amt-2019-405
Preprint. Discussion started: 14 November 2019

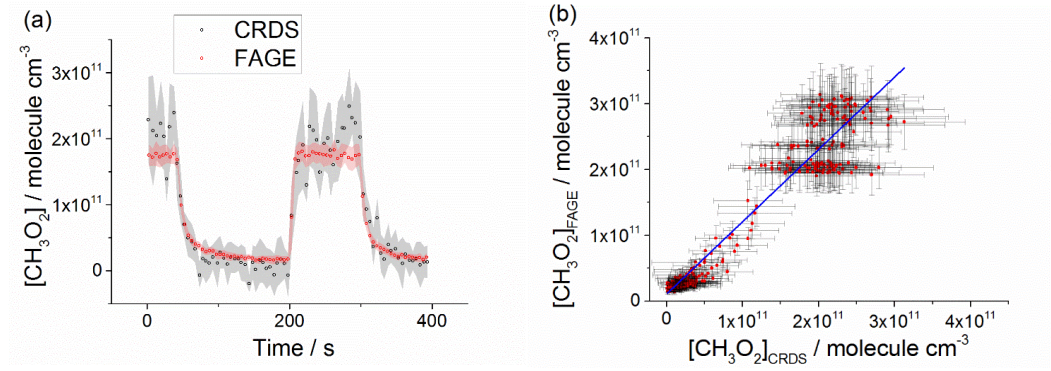

Figure 8. (a) Comparison of CH_3O_2 measurement at 1000 mbar of synthetic air where the lamps were turned off at t ~ 40 s and then on at t ~ 200 s for ~ 2 min before being switched off again. The measurement by FAGE is shown in red and the measurement by CRDS is plotted in black. CH_3O_2 radicals were generated using the 254 nm photolysis of $(CH_3)_2CO$ (8.8×10^{14} molecule cm^{-3}). The 1σ statistical errors generated by the data averaging are shown as grey (CRDS) and red (FAGE) shadows. (b) Correlation plot of all the data generated at 1000 mbar of air. $[CH_3O_2]$ measured by FAGE is plotted against $[CH_3O_2]$ measured by CRDS. The linear fit to the data is generated using the orthogonal distance regression algorithm and results in a gradient of 1.09 ± 0.06 and an intercept of $(1.1 \pm 0.3) \times 10^{10}$ molecule cm^{-3}; fit errors given at 2σ level. In both panels $[CH_3O_2]_{FAGE}$ was determined using a calibration factor of 9.81×10^{-10} counts cm^3 molecule^{-1} s^{-1} mW^{-1} and $[CH_3O_2]_{CRDS}$ was calculated using a cross section of 1.49×10^{-20} cm^2 molecule^{-1}. Each point is an averaged value over 5 s.

4 Conclusions

An intercomparison between the recently developed indirect method for the measurement of the CH_3O_2 radicals using Fluorescence Assay by Gas Expansion (FAGE) (Onel et al., 2017b) and the direct Cavity Ring-Down Spectroscopy (CRDS) method has been performed within the Leeds Highly Instrumented Reactor for Atmospheric Chemistry (HIRAC). CRDS detected CH_3O_2 by using the $A \leftarrow X$ (ν_{12}) electronic transition at 7488 cm^{-1}. The CH_3O_2 radical was generated from the photolysis of mixtures of either $Cl_2/CH_4/O_2$ or acetone//O_2 at room temperature and three total pressures, 80 mbar of He:O_2 = 3:1 and 100 and 1000 mbar of N_2:O_2 = 4:1, and was measured simultaneously using the two methods.

At all pressures FAGE was calibrated using the kinetics of the CH_3O_2 second-order decay by self–reaction. At 1000 mbar the conventional 185 nm photolysis of water vapour in the presence of excess of CH_4 and O_2 was used to calibrate FAGE in addition to the kinetic method. The two calibration methods have overlapping error limits at 2σ level (34% for the water vapour photolysis method and 26% for the kinetic method) as it has been found previously (Onel et al., 2017b). The difference between $C_{CH_3O_2}$(water vapour method) and $C_{CH_3O_2}$(kinetic method) has been discussed in detail previously (Onel et al., 2017b). In the case of HO_2, a very good agreement (difference within 8%) between C_{HO_2}(water vapour method) and C_{HO_2}(kinetic method) was obtained previously (Onel et al., 2017a; Winiberg et al., 2015), which suggests that the production of OH and HO_2 from the photolysis of water vapour in air can be quantified robustly. We consider it unlikely that there is a significant error in the fraction of OH which is converted to CH_3O_2 upon the addition of methane. We consider instead that the discrepancy between the two calibration methods is due to an overestimation of the reported value of k_{obs} for the CH_3O_2 self-reaction (Atkinson et al., 2006); the two methods of calibrations agree if k_{obs} is reduced by 25–30%, which is close to the reported 2σ uncertainty in the rate coefficient (Atkinson et al., 2006). The average value of the sensitivity factor obtained from the two calibration methods, $\overline{C}_{CH_3O_2}$ = $(9.81 \pm 2.03) \times 10^{-10}$ counts cm^3 molecule^{-1} s^{-1} mW^{-1}, corresponds to a limit of detection (*LOD*) for CH_3O_2 of 1.18×10^8 molecule cm^{-3} for a *S*/*N* of 2 and 60 s averaging period. The FAGE sensitivity factor increased by ~3 times by decreasing the pressure in the FAGE detection cell (from 3.3 to 0.9 mbar corresponding to a total HIRAC pressure of 1000 and 100 or 80 mbar, respectively).

https://doi.org/10.5194/amt-2019-405
Preprint. Discussion started: 14 November 2019

Atmospheric Measurement Techniques Discussions

The CH_3O_2 absorption cross section at 7488 cm^{-1} at 100 mbar of air and 80 mbar of $He:O_2$ = 3:1 was determined using the kinetics of the CH_3O_2 second–order decays: σ_{CH3O2} = (1.49 ± 0.19) × 10^{-20} cm^2 $molecule^{-1}$. No change in the shape of the CH_3O_2 spectrum with pressure was found from the reduced pressures (100 mbar of air and 80 mbar of $He:O_2$ = 3:1) to 1000 mbar of air, showing that σ_{CH3O2} is almost independent of pressure. For a time averaging of 60 s the calculated CRDS *LOD* using the Allan-Werle deviation plots and σ_{CH3O2} is around 8 × 10^9 molecule cm^{-3} using acetone/O_2/254 nm at all operating pressures and 6 × 10^9 molecule cm^{-3} using CH_4/Cl_2/black lamps at the reduced pressures.

The FAGE–CRDS intercomparison used measurements of CH_3O_2 under steady-state conditions (photolysis lamps on) as well as rapid decays in [CH_3O_2] (lamps switched off) to cover large concentration ranges: 2–26 × 10^{10} molecule cm^{-3} at 80 mbar of He + O_2 mixture, 2–60 × 10^{10} molecule cm^{-3} at 100 mbar of air and 2–30 × 10^{10} molecule cm^{-3} at 1000 mbar of air. A good agreement between $[CH_3O_2]_{FAGE}$ and $[CH_3O_2]_{CRDS}$ was obtained under all conditions as shown by the gradient of the correlation plots: 1.03 ± 0.05 at 80 mbar He/O_2, 0.95 ± 0.02 at 100 mbar air and 1.09 ± 0.06 at 1000 mbar air (using an average of the sensitivity factors for the two FAGE calibration methods). The study provides a validation for the indirect FAGE method for CH_3O_2 measurements, in agreement with the previous FAGE validation for HO_2 measurements (Onel et al., 2017a).

Data availability. Data presented in this study are available from the authors upon request (chmlo@leeds.ac.uk and d.e.heard@leeds.ac.uk).

Competing interests. The authors declare that they have no conflict of interest.

Acknowledgements

This work has received funding from the Natural Environment Research Council (NERC grant number NE/M011208/1), the National Centre for Atmospheric Science and the European Union's Horizon 2020 research and innovation programme through the EUROCHAMP-2020 Infrastructure Activity under grant agreement No 730997. AB thanks to NERC for a studentship awarded in the framework of the SPHERES doctoral training programme (NE/L002574/1). The authors thank Christa Fittschen for helpful discussions on the absorption cross section of CH_3O_2.

References

Assaf, E., Sheps, L., Whalley, L., Heard, D., Tomas, A., Schoemaecker, C., and Fittschen, C.: The reaction between CH_3O_2 and OH radicals: product yields and atmospheric implications, Environmental Science & Technology, 51, 2170-2177, 10.1021/acs.est.6b06265, 2017.

Atkinson, D. B., and Spillman, J. L.: Alkyl peroxy radical kinetics measured using near infrared CW-cavity ring-down spectroscopy, J. Phys. Chem. A, 106, 8891-8902, 10.1021/jp0257597, 2002.

Atkinson, R., Baulch, D. L., Cox, R. A., Crowley, J. N., Hampson, R. F., Hynes, R. G., Jenkin, M. E., Rossi, M. J., and Troe, J.: Evaluated kinetic and photochemical data for atmospheric chemistry: Volume II - gas phase reactions of organic species, Atmos. Chem. Phys., 6, 3625-4055, 2006.

Cantrell, C. A., Stedman, D. H., and Wendel, G. J.: Measurement of atmospheric peroxy-radicals by chemical amplification, Anal. Chem., 56, 1496-1502, 10.1021/ac00272a065, 1984.

Cantrell, C. A., Zimmer, A., and Tyndall, G. S.: Absorption cross sections for water vapor from 183 to 193 nm (vol 24, pg 2195, 1997), Geophysical Research Letters, 24, 2687-2687, 10.1029/97gl02803, 1997.

Chung, C. Y., Cheng, C. W., Lee, Y. P., Liao, H. Y., Sharp, E. N., Rupper, P., and Miller, T. A.: Rovibronic bands of the A <-X transition of CH_3OO and CD_3OO detected with cavity ringdown absorption near 1.2-1.4 μm, J. Chem. Phys., 127, 10.1063/1.2747616, 2007.

Creasey, D. J., Heard, D. E., and Lee, J. D.: Absorption cross-section measurements of water vapour and oxygen at 185 nm. Implications for the calibration of field instruments to measure OH, HO_2 and RO_2 radicals, Geophysical Research Letters, 27, 1651-1654, 10.1029/1999gl011014, 2000.

Farago, E. P., Viskolcz, B., Schoemaecker, C., and Fittschen, C.: Absorption Spectrum and Absolute Absorption Cross Sections of CH_3O_2 Radicals and CH_3I Molecules in the Wavelength Range 7473-7497 cm^{-1}, J. Phys. Chem. A, 117, 12802-12811, 10.1021/jp408686s, 2013.

Fittschen, C., Whalley, L. K., and Heard, D. E.: The Reaction of CH_3O_2 Radicals with OH Radicals: A Neglected Sink for CH_3O_2 in the Remote Atmosphere, Environmental Science & Technology, 48, 7700-7701, 10.1021/es502481q, 2014.

Fittschen, C.: The reaction of peroxy radicals with OH radicals, Chem.Phys.Lett., 725, 102–108, 2019.

Fuchs, H., Holland, F., and Hofzumahaus, A.: Measurement of tropospheric RO_2 and HO_2 radicals by a laser-induced fluorescence instrument, Rev. Sci. Instrum., 79, 12, 10.1063/1.2968712, 2008.

Glowacki, D. R., Goddard, A., Hemavibool, K., Malkin, T. L., Commane, R., Anderson, F., Bloss, W. J., Heard, D. E., Ingham, T., Pilling, M. J., and Seakins, P. W.: Design of and initial results from a Highly Instrumented Reactor for Atmospheric Chemistry (HIRAC), Atmospheric Chemistry and Physics, 7, 5371-5390, 2007.

https://doi.org/10.5194/amt-2019-405
Preprint. Discussion started: 14 November 2019

Atmospheric Measurement Techniques Discussions

Gordon, I. E., Rothman, L. S., Hill, C., Kochanov, R. V., Tan, Y., Bernath, P. F., Birk, M., Boudon, V., Campargue, A., Chance, K. V., Drouin, B. J., Flaud, J. M., Gamache, R. R., Hodges, J. T., Jacquemart, D., Perevalov, V. I., Perrin, A., Shine, K. P., Smith, M. A. H., Tennyson, J., Toon, G. C., Tran, H., Tyuterev, V. G., Barbe, A., Csaszar, A. G., Devi, V. M., Furtenbacher, T., Harrison, J. J., Hartmann, J. M., Jolly, A., Johnson, T. J., Karman, T., Kleiner, I., Kyuberis, A. A., Loos, J., Lyulin, O. M., Massie, S. T., Mikhailenko, S. N., Moazzen-Ahmadi, N., Muller, H. S. P., Naumenko, O. V., Nikitin, A. V., Polyansky, O. L., Rey, M., Rotger, M., Sharpe, S. W., Sung, K., Starikova, E., Tashkun, S. A., Vander Auwera, J., Wagner, G., Wilzewski, J., Wcislo, P., Yu, S., and Zak, E. J.: The HITRAN2016 molecular spectroscopic database, Journal of Quantitative Spectroscopy & Radiative Transfer, 203, 3-69, 10.1016/j.jqsrt.2017.06.038, 2017.

Green, T. J., Reeves, C. E., Fleming, Z. L., Brough, N., Rickard, A. R., Bandy, B. J., Monks, P. S., and Penkett, S. A.: An improved dual channel PERCA instrument for atmospheric measurements of peroxy radicals, J. Environ. Monitor., 8, 530-536, 10.1039/b514630e, 2006.

Hanke, M., Uecker, J., Reiner, T., and Arnold, F.: Atmospheric peroxy radicals: ROXMAS, a new mass-spectrometric methodology for speciated measurements of HO_2 and ΣRO_2 and first results, Int. J. Mass Spectrom., 213, 91-99, 10.1016/s1387-3806(01)00548-6, 2002.

Hernandez, M. D. A., Burkert, J., Reichert, L., Stobener, D., Meyer-Arnek, J., Burrows, J. P., Dickerson, R. R., and Doddridge, B. G.: Marine boundary layer peroxy radical chemistry during the AEROSOLS99 campaign: Measurements and analysis, J. Geophys. Res.-Atmos., 106, 20833-20846, 10.1029/2001jd900113, 2001.

Huang, D. R., Chu, L. K., and Lee, Y. P.: Infrared absorption of gaseous CH_3OO detected with a step-scan Fourier-transform spectrometer, J. Chem. Phys., 127, 10.1063/1.2807241, 2007.

Jenkin, M. E., Cox, R. A., Hayman, G. D., and Whyte, L. J.: Kinetic study of the reactions CH_3O_2 + CH_3O_2 and CH_3O_2 + HO_2 using molecular modulation spectroscopy, J. Chem. Soc. Faraday Trans. II, 84, 913-930, 10.1039/f29888400913, 1988.

Kline, N. D., and Miller, T. A.: Observation of the A - X electronic transition of C6 - C10 peroxy radicals, Chem. Phys. Lett., 601, 149-154, 10.1016/j.cplett.2014.03.087, 2014.

Kurylo, M. J., and Wallington, T. J.: The temperature dependence of the rate constant for the gas phase disproportionation reaction of CH_3O_2 radicals, Chem. Phys. Lett., 138, 543-547, 10.1016/0009-2614(87)80121-5, 1987.

McAdam, K., Veyret, B., and Lesclaux, R.: UV absorption spectra of HO_2 and CH_3O_2 radicals and the kinetics of their mutual reactions ant 298 K, Chem. Phys. Lett., 133, 39-44, 10.1016/0009-2614(87)80049-0, 1987.

Miyazaki, K., Parker, A. E., Fittschen, C., Monks, P. S., and Kajii, Y.: A new technique for the selective measurement of atmospheric peroxy radical concentrations of HO_2 and RO_2 using a denuding method, Atmos. Meas. Tech., 3, 1547-1554, 10.5194/amt-3-1547-2010, 2010.

Onel, L., Brennan, A., Gianella, M., Ronnie, G., Aguila, A. L., Hancock, G., Whalley, L., Seakins, P. W., Ritchie, G. A. D., and Heard, D. E.: An intercomparison of HO_2 measurements by fluorescence assay by gas expansion and cavity ring-down spectroscopy within HIRAC (Highly Instrumented Reactor for Atmospheric Chemistry), Atmos. Meas. Tech., 10, 4877-4894, 10.5194/amt-10-4877-2017, 2017a.

Onel, L., Brennan, A., Seakins, P. W., Whalley, L., and Heard, D. E.: A new method for atmospheric detection of the CH_3O_2 radical, Atmos. Meas. Tech., 10, 3985-4000, 10.5194/amt-10-3985-2017, 2017b.

Orlando, J. J., and Tyndall, G. S.: Laboratory studies of organic peroxy radical chemistry: an overview with emphasis on recent issues of atmospheric significance, Chem. Soc. Rev., 41, 8213-8213, 2012.

Pushkarsky, M. B., Zalyubovsky, S. J., and Miller, T. A.: Detection and characterization of alkyl peroxy radicals using cavity ringdown spectroscopy, J. Chem. Phys., 112, 10695-10698, 10.1063/1.481705, 2000.

Sander, S. P., and Watson, R. T.: Kinetic studies of the reactions of CH_3O_2 with NO, NO_2 and CH_3O_2 at 298 K, J. Phys. Chem., 84, 1664-1674, 10.1021/j100450a002, 1980.

Sander, S. P., and Watson, R. T.: Temperature dependence of the self-reaction of CH_3O_2 radicals, J. Phys. Chem., 85, 2960-2964, 10.1021/j150620a023, 1981.

Sharp, E. N., Rupper, P., and Miller, T. A.: The structure and spectra of organic peroxy radicals, Phys. Chem. Chem. Phys., 10, 3955-3981, 10.1039/b800954f, 2008.

Simon, F. G., Schneider, W., and Moortgat, G. K.: UV absorption spectrum of the methylperoxy radical and the kinetics of its disproportionation reaction at 300 K, Int. J. Chem. Kinet., 22, 791-812, 10.1002/kin.550220802, 1990.

Sprague, M. K., Mertens, L. A., Widgren, H. N., Okumura, M., Sander, S. P., and McCoy, A. B.: Cavity Ringdown Spectroscopy of the Hydroxy Methyl Peroxy Radical, J. Phys. Chem. A, 117, 10006-10017, 10.1021/jp400390y, 2013.

Tyndall, G. S., Cox, R. A., Granier, C., Lesclaux, R., Moortgat, G. K., Pilling, M. J., Ravishankara, A. R., and Wallington, T. J.: Atmospheric chemistry of small organic peroxy radicals, J. Geophys. Res. -Atmos., 106, 12157-12182, 10.1029/2000jd900746, 2001.

Wallington, T. J., Dagaut, P., and Kurylo, M. J.: Ultraviolet absorption cross-sections and reaction kinetics and mechanisms for peroxy radicals in the gas-phase, Chem. Rev., 92, 667-710, 10.1021/cr00012a008, 1992.

Werle, P., Mucke, R., and Slemr, F.: The limits of signal averaging in atmospheric trace-gas monitoring by tunable diode-laser absorption-spectroscopy (TDLAS), Applied Physics B-Photophysics and Laser Chemistry, 57, 131-139, 10.1007/bf00425997, 1993.

Whalley, L. K., Furneaux, K. L., Goddard, A., Lee, J. D., Mahajan, A., Oetjen, H., Read, K. A., Kaaden, N., Carpenter, L. J., Lewis, A. C., Plane, J. M. C., Saltzman, E. S., Wiedensohler, A., and Heard, D. E.: The chemistry of OH and HO_2 radicals in the boundary layer over the tropical Atlantic Ocean, Atmos. Chem. Phys., 10, 1555-1576, 10.5194/acp-10-1555-2010, 2010.

Whalley, L. K., Edwards, P. M., Furneaux, K. L., Goddard, A., Ingham, T., Evans, M. J., Stone, D., Hopkins, J. R., Jones, C. E., Karunaharan, A., Lee, J. D., Lewis, A. C., Monks, P. S., Moller, S. J., and Heard, D. E.: Quantifying the magnitude of a missing hydroxyl radical source in a tropical rainforest, Atmos. Chem. Phys., 11, 7223-7233, 10.5194/acp-11-7223-2011, 2011.

Whalley, L. K., Blitz, M. A., Desservettaz, M., Seakins, P. W., and Heard, D. E.: Reporting the sensitivity of laser-induced fluorescence instruments used for HO_2 detection to an interference from RO_2 radicals and introducing a novel approach that enables HO_2 and certain RO_2 types to be selectively measured, Atmos. Meas. Tech., 6, 3425-3440, 10.5194/amt-6-3425-2013, 2013.

Whalley, L. K., Stone, D., Dunmore, R., Hamilton, J., Hopkins, J. R., Lee, J. D., Lewis, A. C., Williams, P., Kleffmann, J., Laufs, S., Woodward-Massey, R., and Heard, D. E.: Understanding in situ ozone production in the summertime through radical observations and modelling studies during the Clean air for London project (ClearfLo), Atmos. Chem. Phys., 18, 2547-2571, 10.5194/acp-18-2547-2018, 2018.

Winiberg, F. A. F., Smith, S. C., Bejan, I., Brumby, C. A., Ingham, T., Malkin, T. L., Orr, S. C., Heard, D. E., and Seakins, P. W.: Pressure-dependent calibration of the OH and HO_2 channels of a FAGE HOx instrument using the Highly Instrumented Reactor for Atmospheric Chemistry (HIRAC), Atmos. Meas. Tech., 8, 523-540, 10.5194/amt-8-523-2015, 2015.

Wood, E. C., Deming, B. L., and Kundu, S.: Ethane-Based Chemical Amplification Measurement Technique for Atmospheric Peroxy Radicals, Environ. Sci. Technol. Lett., 4, 15-19, 10.1021/acs.estlett.6b00438, 2017.

Zador, J., Taatjes, C. A., and Fernandes, R. X.: Kinetics of elementary reactions in low-temperature autoignition chemistry, Prog. Energ. Combust., 37, 371-421, 10.1016/j.pecs.2010.06.006, 2011.